Article

Chinese Science Bulletin

Physical Chemistry

October 2010 Vol.55 No.30: 3472–3478
doi: 10.1007/s11434-010-4054-y

One-pot synthesis of PVP-coated $Ni_{0.6}Fe_{2.4}O_4$ nanocrystals

LU XianYong[1,2], NIU Mu[1], YANG ChunHui[1], YI LuoXin[1], QIAO RuiRui[1], DU MeiHong[3] & GAO MingYuan[1*]

[1] *Institute of Chemistry, Chinese Academy of Sciences, Beijing 100190, China;*
[2] *School of Chemistry and Environment, Beijing University of Aeronautics and Astronautics, Beijing 100191, China;*
[3] *Beijing Center for Physical and Chemical Analysis, Beijing 100089, China*

Received January 4, 2010; accepted April 27, 2010

Novel poly(N-vinyl-2-pyrrolidone) (PVP)-coated nickel ferrite nanocrystals were prepared by simultaneously pyrolyzing nickel(II) acetylacetonate ($Ni(acac)_2$) and iron(III) acetylacetonate ($Fe(acac)_3$) in N-vinyl-2-pyrrolidone (NVP). The PVP coating was formed *in situ* through polymerization of NVP. The crystalline structure of the resultant nickel ferrite was analyzed by high-resolution transmission electron microscopy, electron diffraction patterns, and powder X-ray diffraction. In addition, the valence state of Ni and the metal contents of Ni and Fe in different valence states were analyzed by X-ray photoelectron spectroscopy (XPS), atomic absorption and the phenanthroline method. The surface coating layer of PVP and its binding states were characterized by Fourier transform infrared spectroscopy in combination with XPS. Colloidal stability experiments revealed that the nanocrystals could be dispersed well in both phosphate-buffered saline and Dulbecco's Modified Eagle Medium.

magnetic nanocrystals, thermal decomposition, N-vinyl-2-pyrrolidone, colloidal stability

Citation: Lu X Y, Niu M, Yang C H, et al. One-pot synthesis of PVP-coated $Ni_{0.6}Fe_{2.4}O_4$ nanocrystals. Chinese Sci Bull, 2010, 55: 3472–3478, doi: 10.1007/s11434-010-4054-y

Nanocrystals of magnetic ferrites, i.e. $M_xFe_{3-x}O_4$ (M = Fe, Mn, Co, Ni, Zn; $0 \leqslant x \leqslant 1$), have recently received extensive attention because of their potential application in hyperthermia treatment [1–3], magnetic data storage [4], catalysis [5], magnetic resonance imaging (MRI) as contrast agents [6–10], and microwave devices [11]. As a soft magnetic n-type semiconducting material with a fully inverse spinel structure, nickel ferrite is an important member of the spinel family [12–14]. The special physical properties of low magnetic coercivity and high electrical resistivity make nickel ferrite an excellent core material for power transformers in electronic and telecommunication applications [15]. Different synthetic methods such as mechanosynthesis [16], hydrothermal synthesis [17], coprecipitation [18], combustion synthesis [19], sol-gel methods [20], microwave processing [21], and thermal decomposition [10,22], have been used so far to produce nickel ferrite nanocrystals. Among these methods, thermal decomposition of organic metal precursors in high boiling point solvents has been demonstrated as a reliable route for preparing ferrite nanocrystals with uniform size, a high degree of crystallinity, and a clearly defined phase structure [10,23,24].

A thermal decomposition reaction system typically contains three components: a high boiling point solvent, an organic metal precursor and a surface capping agent. For example, Sun et al. [24] reported the synthesis of monodisperse ferrite nanoparticles using benzyl ether as a solvent, metal acetylacetonate complexes as an organic metal precursor, and oleic acid and oleylamine as surface ligands. Cheon et al. reported the preparation of ferrite nanoparticles by a similar method, which involved a high-temperature reaction between a divalent metal chloride (MCl_2, M=Mn, Fe, Co, or Ni) and iron tris-2,4-pentadionate in the presence of oleic acid and oleylamine as surfactants [9]. Bao et al. [22] also succeeded in preparing high quality ferrite nanoparticles by thermolysis of a M^{2+} Fe_2^{3+}-oleate complex

*Corresponding author (email: gaomy@iccas.ac.cn)

(M=Fe, Co, Ni) dissolved in 1-octadecene at 300°C in the presence of oleic acid. Although short chain fatty acids and amines have also been found useful for controlling the synthesis of ferrite nanoparticles [25], they possess quite similar surface properties to the resulting nanoparticles. Therefore, the surface functionalization of ferrite nanoparticles using polymers containing various types of functional groups appeared as an alternative way of producing magnetic nanoparticles with different surface properties, which greatly broadened their potential applications [26,27]. In general, the polymer coating can be realized either by (1) pyrolyzing the metal precursors in the presence of polymers containing functional groups which can anchor onto the surface of the resultant particles [6,7], or (2) performing thermal decomposition in a coordinating solvent with polymerizable properties [28]. Pyrolysis of ferric triacetylacetonate ($Fe(acac)_3$) in N-vinyl-2-pyrrolidone (NVP) is a good example of the latter approach, producing poly(N-vinyl-2-pyrrolidone)-coated magnetic nanoparticles with a greatly simplified reaction system. In this reaction system, NVP was not only used as a coordinating solvent, but also as a radical monomer for the *in situ* formation of a surface coating of poly(N-vinyl-2-pyrrolidone) (PVP). $Fe(acac)_3$ acted as both an iron precursor and as a polymerization initiator. The resulting PVP coating enabled the magnetite nanocrystals obtained to be dispersed in ten different types of organic solvents as well as in aqueous solutions of different pH with very little variation in the hydrodynamic sizes of the particles [28]. Such dispersibility in liquid media is greatly desirable for various applications of nanoparticles.

Following on from our previous investigations, the synthetic method mentioned above was extended further to prepare PVP-coated nickel ferrite nanocrystals by simultaneously pyrolyzing $Ni(acac)_2$ and $Fe(acac)_3$ in NVP. Herein, we report the preparation and crystalline structure of the resultant nickel ferrite nanocrystals, as well as discussing the reaction mechanism.

1 Materials and methods

1.1 Materials

$Fe(acac)_3$ and $Ni(acac)_2$ were purchased from Aldrich (14024-18-1, 97%; 3264-82-2, 95%, respectively) and used after recrystallizing twice. Medical grade NVP was obtained from Jiaozuo Meida Fine Chemical Co., Ltd and purified by distillation under reduced pressure in the presence of phenothiazine. All other chemicals were of analytical grade and were used as received.

1.2 Synthesis of nickel ferrite nanocrystals

Nickel ferrite nanocrystals were synthesized by pyrolyzing $Fe(acac)_3$ and $Ni(acac)_2$ in NVP at 200°C. In a typical preparation, $Fe(acac)_3$ and $Ni(acac)_2$ were first dissolved in NVP with a molar ratio of 2∶1. The total concentration of metal (Fe, Ni) precursors was 0.06 mol/L. The solution was purged with argon for 30 minutes at room temperature to remove oxygen, and subsequently heated to 200°C under argon. Aliquots were extracted from the reaction mixture at 1, 2, 4 and 6 h, and denoted as samples A, B, C and D, respectively. The nanocrystals were purified as follows. First, equal volumes of ethanol were introduced into the aliquots extracted at different times. Five times this volume of diethyl ether was then added to induce precipitation. The resulting black precipitates were then isolated using a permanent magnet. The nanocrystal samples were obtained by repeating this precipitation procedure three times.

To reveal that nickel ferrite nanoparticles had formed, the thermal decomposition of $Ni(acac)_2$ in NVP was also investigated. The reaction procedure was generally the same as that for the nickel ferrite nanocrystals. First, $Ni(acac)_2$ was dissolved in NVP to give a 0.04 mol/L solution. The resulting light-green transparent solution was purged with argon gas for 30 min at room temperature to remove oxygen, and then heated to 200°C. The color of the reaction mixture turned from light-green to black during the heating process. The reaction typically finished within 1 h at 200°C. The resulting nanoparticles were purified by the procedure described above.

1.3 Characterization

Transmission electron microscope (TEM) and electron diffraction (ED) measurements were performed on a JEM-100CXII electron microscope at an acceleration voltage of 100 kV. High-resolution TEM (HRTEM) images were taken on a JEM-2100F microscope at an accelerating voltage of 200 kV. Energy-dispersive X-ray spectroscopy (EDXS) was carried out using a GENESIS system (EDAX Inc.) attached to a TEM. The content of Fe and Ni in the nanoparticle samples were analyzed on a PerkinElmer AAnalyst™ 800 high-performance atomic absorption spectrometer (AAS) equipped with a high performance burner system. Elemental Fe and Ni were detected at 248.3 nm and 232.0 nm, respectively, with single element hollow cathode lamps. The spectral bandwidth for all of the element detections was set as 0.7 nm. The molar ratio of Fe(III) and Fe(II) was determined by the phenanthroline method [29]. Powder X-ray diffraction (XRD) measurements were preformed on a Rigaku D/Max-2500 diffractometer with Cu $K\alpha_1$ radiation (λ = 1.54056 Å). The hydrodynamic diameter of the magnetic nanocrystals was determined with a Malvern Zetasizer (Nano ZS). Fourier transform infrared spectroscopy (FTIR) was performed on a Bruker EQUINOX55 FTIR spectrometer under ambient conditions. X-ray photoelectron spectroscopy (XPS) data were obtained with an ESCALab220i-XL electron spectrometer from VG Scientific using 300 W Mg Kα radiation. The base pressure was about 3×10^{-9} mbar. Thermogravimetric analysis (TGA) was car-

ried out on a PerkinElmer Pyris 1 analyzer. The temperature range was set between 20 and 850°C with a temperature increase rate of 10°C/min under a nitrogen atmosphere. The magnetic properties of the samples were characterized by a vibrating sample magnetometer (VSM, JDM-13, China).

2 Results

Figure 1 shows TEM images of samples A-D. The four samples generally contain quasispherical nanoparticles with average diameters that increase slightly with reaction time, i.e. 4.4±0.9 nm for sample A, 5.1±1.2 nm for sample B, 6.7±1.4 nm for sample C, and 6.7±1.7 nm for sample D. The HRTEM results shown in Figure 2 demonstrate that the quasispherical particles are single crystals with crystal planes that are consistent with those of $Ni_{0.6}Fe_{2.4}O_4$. The electron diffraction results presented in Table 1 reveal that the *d*-spacing values of the nanocrystals closely match those of the JCPDS card for $Ni_{0.6}Fe_{2.4}O_4$ (No. 87-2338), which is consistent with the lattice analysis in Figure 2. The crystalline structure of the nanoparticles was further verified by XRD. The results shown in Figure 3 provide strong evidence that the nanoparticles are composed of $Ni_{0.6}Fe_{2.4}O_4$.

The metal compositions in the samples were analyzed by energy-dispersive X-ray (EDX) spectroscopy. The experimental results shown in Figure S1 of the Supporting Information (SI) demonstrate that the atomic ratio of Ni∶Fe in sample D is 1∶4.0, consistent with the stoichiometric ratio of Fe to Ni in $Ni_{0.6}Fe_{2.4}O_4$. The molar ratios of Ni∶Fe in the other samples, determined by AAS, were 1∶3.7 for sample A, 1∶4.1 for sample B, and 1∶3.7 for sample C, which are also quite close to the theoretical value of 1∶4.

The presence of Ni(II) in the nanoparticles was further verified by XPS analysis. All of the binding energies for Ni 2p, Ni 3p, O 1s, and N 1s were calibrated to C 1s (284.8 eV) of adventitious carbon as a reference. The spectra of Ni 2p and Ni 3p (Figure 4) were fitted using a Shirley-type background. The binding energy of Ni 2p and Ni 3p are 854.5 eV and 67.1 eV, respectively, which demonstrates that Ni mainly exists in the crystal lattice in the form of divalent ions [30–32]. Based on the XPS result, the molar ratio of Ni(II) to Fe(II) in the particles was further determined by AAS in combination with the phenanthroline method to differentiate Fe(II) from Fe(III). The experimentally obtained ratio was 2.2∶1, which is close to the theoretical value of 1.5∶1 for $Ni_{0.6}Fe_{2.4}O_4$ ($Ni^{2+}{}_{0.6}Fe^{2+}{}_{0.4}Fe^{3+}{}_2O^{2-}{}_4$).

Sample D was also characterized by FTIR (Figure 5). Compared with the FTIR spectrum of NVP which shows vibrational peaks of the vinyl group at 1630 cm^{-1} and 983 cm^{-1}, the spectrum of sample D lacks these signals, which suggests that NVP is polymerized during the reaction to form PVP [33]. The vibrational band from the carbonyl group shifts from 1680 to 1657 cm^{-1} after the reaction. This implies that the resultant PVP is chemically anchored onto the surface of the $Ni_{0.6}Fe_{2.4}O_4$ nanocrystals *via* the carbonyl group of PVP [28,33,34].

The magnetic properties of the as-synthesized nickel ferrite nanocrystals were studied with a VSM. The room temperature magnetization curve shown in Figure 6 demonstrates that the nanoparticles are superparamagnetic with a

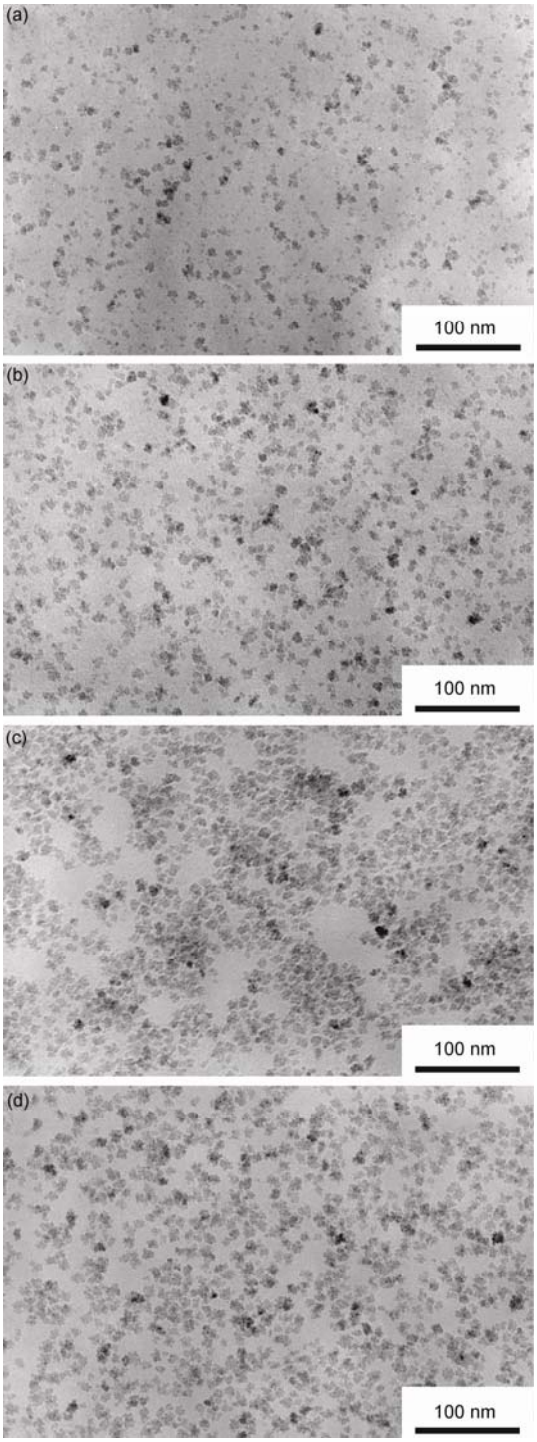

Figure 1 TEM images of sample A (a), sample B (b), sample C (c) and sample D (d).

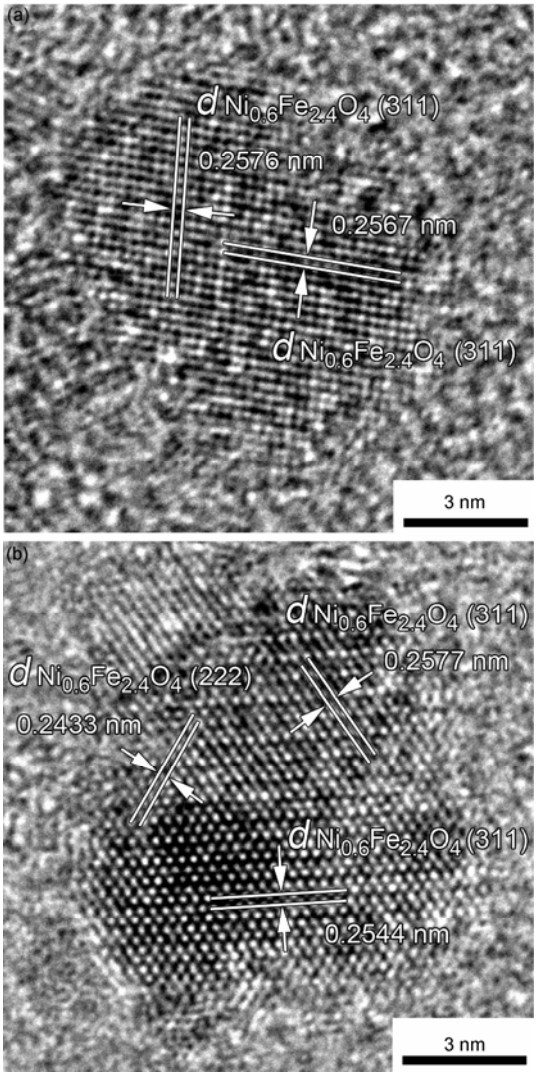

Figure 2 HRTEM images of sample A (a) and sample D (b) overlaid with identification of crystal planes of $Ni_{0.6}Fe_{2.4}O_4$.

Table 1 The *d*-spacing values obtained based on the electron diffraction patterns of samples A–D, together with the data for $Ni_{0.6}Fe_{2.4}O_4$ from JCPDS card no. 87-2338

Sample A	Sample B	Sample C	Sample D	$Ni_{0.6}Fe_{2.4}O_4$	*hkl*
2.9478	2.9843	2.9627	2.9670	2.9559	220
2.5275	2.5590	2.5290	2.5320	2.5208	311
2.0965	2.1029	2.0943	2.0993	2.0902	400
1.7146	1.7211	1.7203	1.7146	1.7066	422
1.6082	1.6120	1.6152	1.6158	1.6090	511
1.4776	1.4744	1.4900	1.4845	1.4779	440
1.2747	1.2863	1.2867	1.2807	1.2750	533

saturation magnetization of 31.1 emu/g. Taking the organic content of sample D (48.8%) determined by TGA into consideration, the saturation magnetization value of pure $Ni_{0.6}Fe_{2.4}O_4$ in sample D is around 60.9 emu/g.

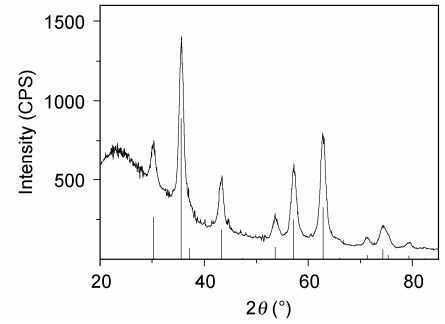

Figure 3 Powder X-ray diffractogram of sample D. The line patterns shown on the bottom are standard data for $Ni_{0.6}Fe_{2.4}O_4$ from JCPDS card 87-2338.

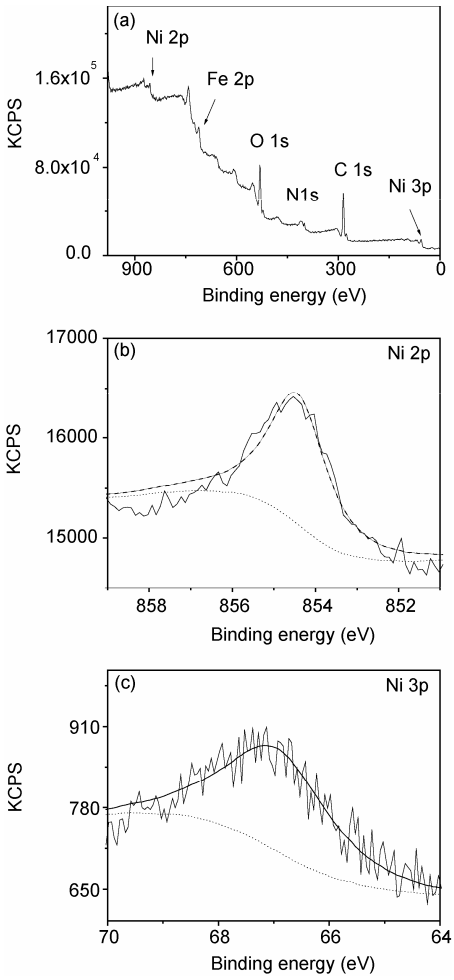

Figure 4 X-ray photoelectron spectrum of sample D (a), and high resolution spectra of Ni 2p (b) and Ni 3p (c).

3 Discussion

As demonstrated above, the preparation used led to $Ni_{0.6}Fe_{2.4}O_4$ nanocrystals independent of the reaction time between 1 and 6 h. The atomic ratio of Ni/Fe in the resultant nanocrystals is dissimilar to the molar ratio of the reactants,

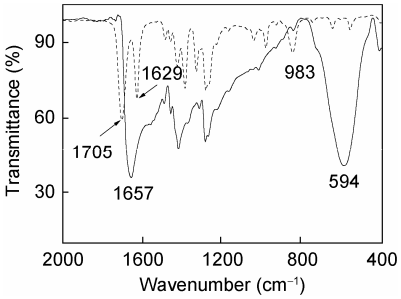

Figure 5 FTIR spectra of NVP (dashed line) and sample D (solid line).

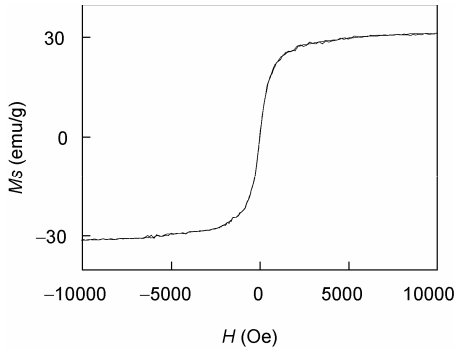

Figure 6 Room temperature magnetization curve of sample D.

i.e. 1∶2, from which $NiFe_2O_4$ was expected according to the literature [9,22]. To further reveal why $Ni_{0.6}Fe_{2.4}O_4$ formed instead of $NiFe_2O_4$, a solution of $Ni(acac)_2$ with a 0.04 mol/L concentration was pyrolyzed in NVP. The thermolysis of $Ni(acac)_2$ gave rise to a large color change from green to black within the first 10 min of reaction at 200°C. Such a color change was not observed when $Fe(acac)_3$ was present in the reaction system. Further TEM and electron diffraction characterization of the black sample collected after 1 h reaction demonstrated that the resultant particles are different from those prepared in the presence of $Fe(acac)_3$. As shown in Figure 7, the average size of the particles is 45.4 nm. The *d*-spacing values calculated from the electron diffraction patterns suggest that the particles are cubic nickel according to standard data from JCPDS card (No. 04-0850). In contrast, nickel particles were not obtained by pyrolyzing $Ni(acac)_2$ in phenyl ether under the same experimental conditions, implying that NVP can reduce Ni(II) at high temperature to form metallic Ni.

Although the details of the thermal decomposition behavior of the metal acetylacetonate complexes in NVP is difficult to observe at high temperature, the experimental results suggest that NVP might reduce $Ni(acac)_2$ to Ni(II) more easily than it reduces $Fe(acac)_3$ to Fe(II). Therefore, a possible mechanism for the formation of $Ni_{0.6}Fe_{2.4}O_4$ ($Ni^{2+}{}_{0.6}Fe^{2+}{}_{0.4}Fe^{3+}{}_2O^{2-}{}_4$) is proposed as follows. In the early stages of the reaction, $Ni(acac)_2$ is quickly decomposed and reduced to form elemental nickel which subsequently reacts with Fe(III), giving rise to both Ni(II) and Fe(II) while the metal oxide particles are formed. As Ni(II) and Fe(II) possess comparable ionic radii [35], they can both enter the crystal lattice, so $Ni_{0.6}Fe_{2.4}O_4$ is formed rather than $NiFe_2O_4$. It is known that Fe(III) can partly be reduced when $Fe(acac)_3$ is pyrolyzed in either 2-pyrolidone [36,37] or N-vinyl-2-pyrolidone [28]. The possible formation of Fe(II) by reaction of elemental Ni with Fe(III) in the early stage of the reaction is more favorable because it is supported by the fact that Ni particles were not found in the reaction system containing both $Ni(acac)_2$ and $Fe(acac)_3$.

The novel $Ni_{0.6}Fe_{2.4}O_4$ nanocrystals possess similar properties to magnetite, making them attractive for biomedical applications [6–10]. Solubility and colloidal stability in water are basic requirements for bioapplications of magnetic nanoparticles [23]. Activity in aqueous media around neutral pH is an important condition for *in vivo* applications to coincide with physiological pH (7.35–7.45 for human blood). Nevertheless, satisfying colloidal stability at neutral pH is not enough for magnetic nanoparticles; biomedical applications require physiological conditions with a 0.17 mol/L ionic strength. Phosphate-buffered saline

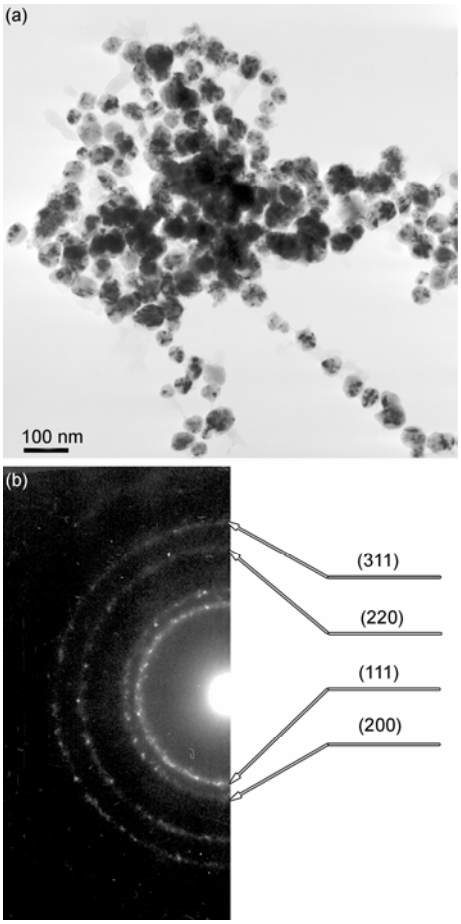

Figure 7 TEM images (a) and electron diffraction patterns (b) of the nanoparticles obtained by pyrolyzing $Ni(acac)_2$ in NVP. The diffraction rings are labeled with the Miller indices of cubic Ni (JCPDS card No. 04-0850).

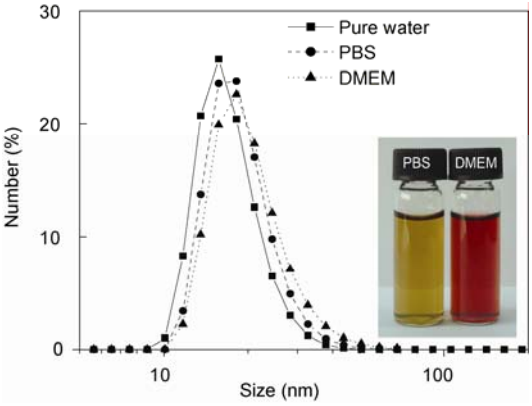

Figure 8 Hydrodynamic size distribution profiles of sample D in pure water, PBS and DMEM (Inset: photographs of sample D in PBS and DMEM).

(PBS) can simulate above-mentioned conditions because its pH and ionic concentration are similar to body fluids. For actual physiological conditions, a variety of proteins should also be taken into consideration besides the pH and ionic strength. Dulbecco's Modified Eagle Medium (DMEM) with a high concentration of glucose is widely employed for supporting the growth of a broad range of mammalian cell lines and can mimic physiological conditions well. Therefore, the colloidal stability of the nickel ferrite nanocrystals was investigated in different types of biological media such as PBS and cell culture media. The hydrodynamic size of sample D in pure water, 1 mol/L PBS buffer and DMEM cell culture medium was determined to be 17.3, 19.0 and 20.6 nm, respectively. Most importantly, the PVP-coated $Ni_{0.6}Fe_{2.4}O_4$ nanocrystals do not agglomerate in either PBS or DMEM cell culture medium (Figure 8), which allows them to be used further in some bioapplications, for example, magnetic labeling of cells.

The excellent water solubility and good colloidal stability of the as-prepared $Ni_{0.6}Fe_{2.4}O_4$ nanocrystals in different solutions that mimic physiological conditions can be attributed to PVP binding to the particle surface as was found in the FTIR investigations. To provide more details about the binding of PVP, the XPS signals of N 1s and O 1s were fitted by multiple Gaussian functions with an equal full width at half-maximum using a Shirley-type background. The results are shown in Figure 9. The binding energy of the N 1s signal of sample D is similar to that of pure PVP [38]. However, the fitting results of the O 1s signal suggest that the O 1s signal is a convolution of three peaks at 529.8, 531.1, and 532.2 eV. According to reference data, these three peaks can be assigned to O from $Ni_{0.6}Fe_{2.4}O_4$ [31], O from PVP [38], and O from PVP coordinating with $Ni_{0.6}Fe_{2.4}O_4$ nanocrystals, respectively [28]. Based on this analysis, the ratio between the coordinating and non-coordinating PVP segments is estimated to be around 1∶3, which explains the excellent colloidal stability of the resultant nanocrystals in PBS and DMEM aqueous solutions. This colloidal stability

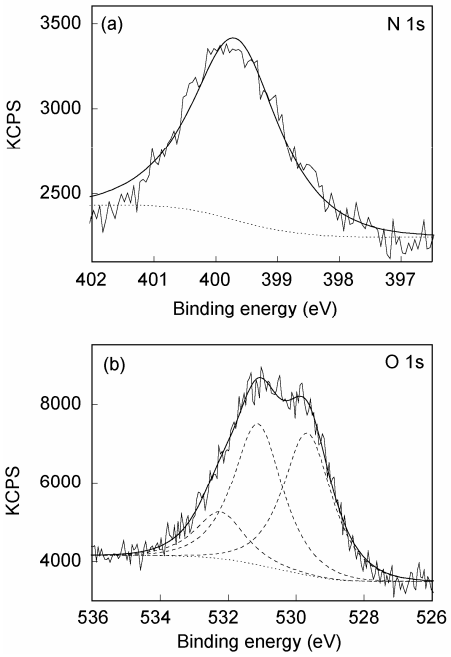

Figure 9 X-ray photoelectron spectra of N 1s (a) and O 1s (b) signals recorded for sample D. The dashed lines are calculated spectra.

arises from the free PVP segments, while the coordinating segments of PVP mainly serve as stabilizing agents, preventing the nanocrystals from uncontrolled growth like the conventional surfactants commonly used in nanocrystal synthesis.

4 Conclusions

In summary, novel PVP-coated nickel ferrite ($Ni_{0.6}Fe_{2.4}O_4$) nanocrystals were prepared in a one-pot reaction by simultaneously decomposing $Ni(acac)_2$ and $Fe(acac)_3$ in NVP at 200°C. In this preparation, NVP was used as a high boiling point coordinating solvent. The polymerizable nature of NVP allowed PVP to be formed *in situ* as a surface coating on the nanocrystals. Systematic investigations were performed to identify the crystalline structure and formation mechanism of this new type of nanocrystal. FTIR and XPS investigations revealed that PVP coordinates on the nickel ferrite nanoparticle surface *via* carbonyl groups. As only one quarter of the PVP segments coordinate to the nanocrystals, the remaining PVP segments offer the nanoparticles excellent colloidal stability in both PBS buffer and DMEM cell culture media, making the particles potentially useful in magnetic cell labeling applications.

This work was supported by the National Natural Science Foundation of China (20640430564 and 20820102035), the Knowledge Innovation Program of the Chinese Academy of Sciences (KJCX2-YW-M15) and the Ministry of Health (2008ZX10001-014).

1 Bae S, Lee S W, Takemura Y. Applications of $NiFe_2O_4$ nanoparticles for a hyperthermia agent in biomedicine. Appl Phys Lett, 2006, 89: 252503
2 Pradhan P, Giri J, Samanta G, et al. Comparative evaluation of heating ability and biocompatibility of different ferrite-based magnetic fluids for hyperthermia application. J Biomed Mater Res B, 2006, 81b: 12–22
3 Kim D H, Nikles D E, Johnson D T, et al. Heat generation of aqueously dispersed $CoFe_2O_4$ nanoparticles as heating agents for magnetically activated drug delivery and hyperthermia. J Magn Magn Mater, 2008, 320: 2390–2396
4 Sugimoto M. The Past, present, and future of ferrites. J Am Ceram Soc, 1999, 82: 269–280
5 Ramankutty C G, Sugunan S. Surface properties and catalytic activity of ferrospinels of nickel, cobalt and copper, prepared by soft chemical methods. Appl Catal A-Gen, 2001, 218: 39–51
6 Li Z, Wei L, Gao M, et al. One-pot reaction to synthesize biocompatible magnetite nanoparticles. Adv Mater, 2005, 17: 1001–1005
7 Hu F, Wei L, Zhou Z, et al. Preparation of biocompatible magnetite nanocrystals for *in vivo* magnetic resonance detection of cancer. Adv Mater, 2006, 18: 2553–2556
8 Song H T, Choi J S, Suh J, et al. Surface modulation of magnetic nanocrystals in the development of highly efficient magnetic resonance probes for intracellular Label. J Am Chem Soc, 2005, 127: 9992–9993
9 Lee J H, Huh Y M, Jun Y, et al. Artificially engineered magnetic nanoparticles for ultra-sensitive molecular imaging. Nat Med, 2007, 13: 95–99
10 Tromsdorf U I, Bigall N C, Kaul M G, et al. Size and surface effects on the MRI relaxivity of manganese ferrite nanoparticle contrast agents. Nano Lett, 2007, 7: 2422–2427
11 Rubinger C P L, Gouveia D X, Nunes J F, et al. Microwave dielectric properties of $NiFe_2O_4$ nanoparticles ferrites. Microw Opt Technol Lett, 2007, 49: 1341–1343
12 Tsukimura K, Sasaki S, Kimizuka N. Cation distributions in nickel ferrites. Jpn J Appl, 1997, 36: 3609–3612
13 Chinnasamy C N, Narayanasamy A, Ponpandian N, et al. Mixed spinel structure in nanocrystalline $NiFe_2O_4$. Phys Rev B, 2001, 63: 184108 1–6
14 Lüders U, Barthélémy A, Bibes M, et al. $NiFe_2O_4$: A versatile spinel material brings new opportunities for spintronics. Adv Mater, 2006, 18: 1733–1736
15 Wang Z L, Liu X J, Lv M F, et al. Preparation of ferrite MFe_2O_4 (M = Co, Ni) ribbons with nanoporous structure and their magnetic properties. J Phys Chem B, 2008, 112: 11292–11297
16 Šepelák V, Bergmann I, Feldhoff A, et al. Nanocrystalline nickel ferrite, $NiFe_2O_4$: Mechanosynthesis, nonequilibrium cation distribution, canted spin arrangement, and magnetic behavior. J Phys Chem C, 2007, 111: 5026–5033
17 Zhou J, Ma J F, Sun C, et al. Low-temperature synthesis of $NiFe_2O_4$ by a hydrothermal method. J Am Ceram Soc, 2005, 88: 3535–3537
18 Albuquerque A S, Ardisson J D, Macedo W A A, et al. Structure and magnetic properties of nanostructured Ni-ferrite. J Magn Magn Mater, 2001, 226: 1379–1381
19 Vivekanandhan S, Venkateswarlu M, Satyanarayana N. Effect of ethylene glycol on polyacrylic acid based combustion process for the synthesis of nano-crystalline nickel ferrite ($NiFe_2O_4$). Mater Lett, 2004, 58: 2717–2720
20 Liu J H, Wang L, Li F S. Magnetic properties and Mossbauer studies of nanosized $NiFe_2O_4$ particles. J Mater Sci, 2005, 40: 2573–2575
21 Komarneni S, D'Arrigo M C, Leionelli C, et al. Microwave-hydrothermal synthesis of nanophase ferrites. J Am Ceram Soc. 1998, 81: 3041–3043
22 Bao N, Shen L, Wang Y, et al. A Facile Thermolysis route to monodisperse ferrite nanocrystals. J Am Chem Soc, 2007, 129: 12374–12375
23 Qiao R R, Yang C H, Gao M Y. Superparamagnetic iron oxide nanoparticles: from preparations to *in vivo* MRI applications. J Mater Chem, 2009, 19: 6274–6293
24 Sun S, Zeng H, Robinson D B, et al. Monodisperse MFe_2O_4 (M = Fe, Co, Mn) nanoparticles. J Am Chem Soc, 2004, 126: 273–279
25 Niederberger M, Pinna N. Metal Oxide Nanoparticles in Organic Solvents. London: Spring, 2009
26 Kim M, Chen Y, Liu Y, et al. Super-stable, high-quality Fe_3O_4 dendron-nanocrystals dispersible in both organic and aqueous solutions. Adv Mater, 2005, 17: 1429–1432
27 Xie J, Xu C, Xu Y, et al. Linking hydrophilic macromolecules to monodisperse magnetite (Fe_3O_4) nanoparticles via trichloro-s-triazine. Chem Mater, 2006, 18: 5401–5403
28 Lu X Y, Niu M, Qiao R R, et al. Superdispersible PVP-Coated Fe_3O_4 nanocrystals prepared by a "one-pot" reaction. J Phys Chem B, 2008, 112: 14390–14394
29 Taras M J, Greenberg A E, Hoak R D, et al. Standard methods for the examination of water and wastewater. Washington DC: Am Public Health Assoc, 1971
30 Kim K S, Baitinger W, Amy J W, et al. ESCA studies of metal-oxygen surfaces using argon and oxygen Ion-bombardmen. J Electron Spectrosc, 1974, 5: 351–367
31 Hirokawa K, Honda F, Oku M. On the surface chemical reactions of metal and oxide XPS samples at 300–400°C at a high vacuum produced by oil diffusion pumps. J Electron Spectrosc, 1975, 6: 333–345
32 McIntyre N S, Cook M G. X-Ray photoelectron studies of some oxides and hydroxides of cobalt, nickel, and copper. Anal Chem, 1975, 47: 2208–2213
33 Doneux C, Caudano R, Delhalle J, et al. Polymerization of N-Vinyl-2-Pyrrolidone under anodic polarization: Characterization of the modified electrode and study of the grafting mechanism. Langmuir, 1997, 13: 4898–4905
34 Nemamcha A, Rehspringer J L, Khatmi D. Synthesis of palladium nanoparticles by sonochemical reduction of palladium(ii) nitrate in aqueous solution. J Phys Chem B, 2006, 110: 383–387
35 Cao X, Song T, Wang X. Inorganic Chemistry. Beijing: Higher Education Press, 2000
36 Li Z, Chen H, Bao H, et al. One-pot reaction to synthesize water-soluble magnetite nanocrystals. Chem Mater, 2004, 16: 1391–1393
37 Li Z, Sun Q, Gao M Y. Preparation of water-soluble Magnetite nanocrystals by refluxing ferric hydrated salts in 2-pyrrolidone: Mechanism leading to Fe_3O_4. Angew Chem Int Ed, 2005, 44: 123–126
38 Beamson G, Briggs D. High Resolution XPS of Organic Polymers: The Scienta Esca300 Database. Chichester: John Wiley & Sons, 1992

Supporting Information

Table S1 TEM image of sample D (a) and EDX spectrum (b) recorded from the particles presented in the black square. The atomic percentages of Fe and Ni elements in given area are provided in the table inserted in frame (b).

The supporting information is available online at csb.scichina.com and www.springerlink.com. The supporting materials are published as submitted, without typesetting or editing. The responsibility for scientific accuracy and content remains entirely with the authors.

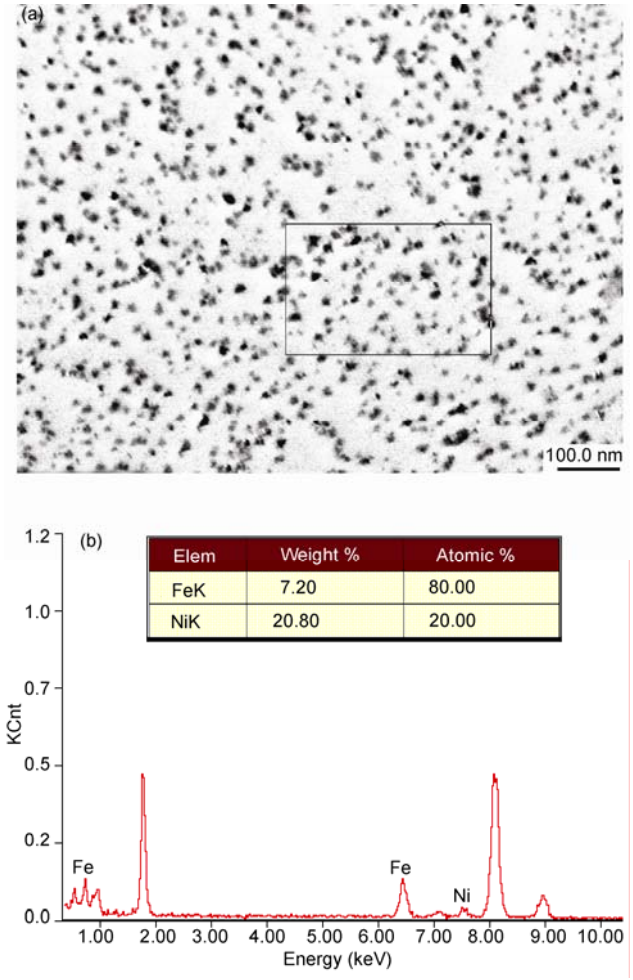

Table S1 TEM image of sample D (a) and EDX spectrum (b) recorded from the particles presented in the black square. The atomic percentages of Fe and Ni elements in given area are provided in the table inserted in frame (b).